The Astrophysical Journal Letters, 943:L27 (5pp), 2023 February 1 https://doi.org/10.3847/2041-8213/acb5f2

Dusty-wind-clear JWST Super-early Galaxies

Fabrizio Fiore[1,2], Andrea Ferrara[3], Manuela, Bischetti[4], Chiara Feruglio[1], and Andrea Travascio[5]
[1] INAF-Osservatorio Astronomico di Trieste, via Tiepolo 11, I-34143 Trieste, Italy; fabrizio.fiore@inaf.it
[2] IFPU—Institute for Fundamental Physics of the Universe, via Beirut 2, I-34151 Trieste, Italy
[3] Scuola Normale Superiore, Piazza dei Cavalieri 7, I-50126 Pisa, Italy
[4] Dipartimento di Fisica, Università di Trieste, Sezione di Astronomia, Via G.B. Tiepolo 11, I-34131 Trieste, Italy
[5] Universitá degli Studi di Milano Bicocca, Piazza dell'Ateneo Nuovo 1, I-20126, Milan, Italy
Received 2022 November 16; revised 2023 January 15; accepted 2023 January 21; published 2023 February 2

Abstract

The JWST discovery of a number of super-early (redshift $z > 10$) blue galaxies requires these systems to be essentially dust free in spite of their large stellar masses. A possible explanation is that dust is evacuated by radiatively driven outflows. We test this hypothesis by deriving the Eddington ratio $\lambda_E = L_{\rm bol}/L_E$, where $L_{\rm bol}$ is the bolometric luminosity produced by star formation and possible black hole accretion, for 134 galaxies at $6.5 < z < 16$. We find a strong anticorrelation between λ_E and dust UV optical depth, $\tau_{1500} \propto \lambda_E^{-0.63}$; also, λ_E increases with redshift. We confirm that galaxies exceeding a specific star formation rate sSFR > 13 Gyr^{-1} develop powerful outflows clearing the galaxy from its dust. This result is supported by ALMA dust continuum nondetections in three super-early systems.

Unified Astronomy Thesaurus concepts: High-redshift galaxies (734); Galaxy evolution (594); Galaxy formation (595)

1. Introduction

The first James Webb Space Telescope (JWST) images of the distant universe are leading to tremendous progress in our understanding of the earliest phases of galaxy evolution. Such super-early (redshift $z \gtrsim 10$) galaxies show a large range of UV luminosities ($L_{\rm UV} = 10^{42}$–10^{46} erg s^{-1}), stellar masses ($M_* \approx 10^{6-10} M_\odot$), star formation rates (SFR $= 0.1$– $300\, M_\odot$ yr^{-1}), and dust optical depths at rest-frame 1500 Å, $\tau_{1500} = 0$–15 (Barrufet et al. 2022; Bradley et al. 2022; Castellano et al. 2022; Curti et al. 2022; Finkelstein et al. 2022; Furtak et al. 2022; Harikane et al. 2022; Leethochawalit et al. 2023; Naidu et al. 2022; Rodighiero et al. 2022; Topping et al. 2022; Trussler et al. 2022; Whitler et al. 2022; Adams et al. 2023).

Remarkably, though, their sizes are quite similar and compact, with optical half-light radii, r_e, of just 0.1–0.5 kpc (Ono et al. 2022; Yang et al. 2022). The corresponding high radiation energy density from bright star-forming sites, and possibly, accreting black holes (BHs), induces a strong radiation pressure on dust and gas. Depending on the Eddington ratio $\lambda_E \equiv L_{\rm bol}/L_E =$ (where $L_{\rm bol}$ is the bolometric luminosity produced by star formation and any possible BH accretion, L_E is the Eddington luminosity) and dust-to-gas ratio, D, radiation-driven dusty outflows might develop. Such outflows remove gas and dust from the galaxy, temporarily quenching its star formation until the next gas accretion event. Dusty outflows have been widely studied in the literature, using analytical, semiempirical, and numerical approaches (Ferrara et al. 1990; Arav et al. 1994; Scoville et al. 2001; Murray et al. 2005; Thompson et al. 2005, 2015; Fabian et al. 2006, 2008; Krumholz & Thompson 2012, 2013; Ricci et al. 2017). The condition for the onset of the outflow can be expressed in terms of an effective Eddington ratio for dust absorption, $\lambda_E^{\rm eff}$, where the optical-UV dust extinction cross section, σ_d, substitutes the Thomson one, σ_T, in the standard L_E definition.

If dust is considered, the radiation pressure efficiency is boosted by a factor $A = L_a/L_{\tau_T} \approx 10^2 - 10^3$, where L_a is the absorbed luminosity for not fully ionized and dusty gas and L_{τ_T} is the absorbed luminosity for a fully ionized gas (e.g., Fabian et al. 2006, 2008). When $\lambda_E > \lambda_E^{\rm eff} = \lambda_E/A$, radiation pressure is capable of expelling dust and gas[6] from the source. Dust ejection by radiation pressure has been indeed invoked by Ziparo et al. (2022) to explain the blue colors of $z > 8$ JWST candidates.

In this Letter, we collect a sample of 134 galaxies at redshift $6.5 < z < 16$, calculate their Eddington ratio and compare it with $\lambda_E^{\rm eff}$. We then interpret high-redshift galaxy observations in the framework of the radiation-driven dusty outflow scenario, expanding on the Ziparo et al. (2022) findings.

2. Sample Selection

We have collected from the recent literature extinction-corrected UV luminosities, SFR, stellar masses, and extinction properties (i.e., τ_{1500}) for a sample of 134 galaxies at $z > 6.5$. These quantities were computed in most cases by fitting the optical and near-IR photometry with a spectral energy distribution (SED) model using the BEAGLE tool (Chevallard & Charlot 2016). In particular, we have used data from Barrufet et al. (2022), Bradley et al. (2022), Castellano et al. (2022), Curti et al. (2022), Finkelstein et al. (2022), Furtak et al. (2022), Harikane et al. (2022), Leethochawalit et al. (2023), Naidu et al. (2022), Rodighiero et al. (2022), Topping et al. (2022), Trussler et al. (2022), and Whitler et al. (2022). We complemented this JWST galaxy sample by the REBELS (Bouwens et al. 2022) and CANDELS Lyα (Endsley et al. 2021) samples.

[6] We assume that dust and gas are strongly coupled by both Coulomb and viscous drag forces.

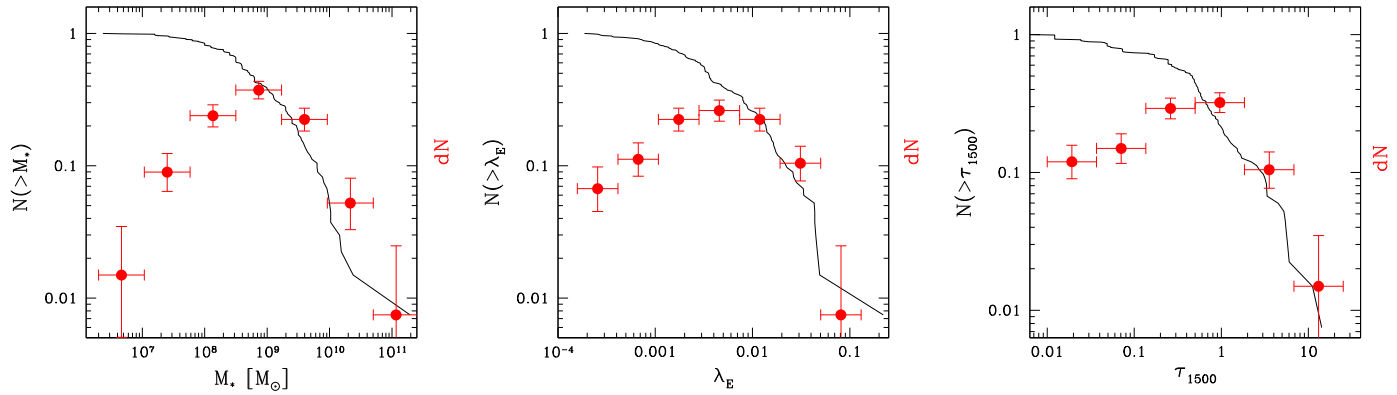

Figure 1. Stellar mass, M_*; Eddington ratio, λ_E; and UV dust optical depth, τ_{1500}; from normalized cumulative (black curves) and differential (red points) distributions for our galaxy sample.

We use published UV luminosities (at 1500 Å, L_{1500}) when available; in the other cases, these are obtained via the relation[7] $L_{1500} = 2.2 \times 10^{43}\,(\mathrm{SFR}/M_\odot\,\mathrm{yr}^{-1})$ [erg s^{-1}], assuming a Kroupa stellar IMF with constant SFR over 100 Myr. We use τ_{1500} when available, or obtain it from UV β slopes as $\tau_{1500} = \beta - \beta_{\rm int}$, with $\beta_{\rm int} = -2.616$ (Reddy et al. 2018), otherwise. From the definition $L_E = 4\pi G\, m_p\, c\, M_*/\sigma_T = 1.26 \times 10^{38} (M_*/M_\odot)$ erg s^{-1}, we compute the Eddington ratio as $\lambda_E = L_{\rm bol}/L_E$ by further assuming a bolometric correction, $f_{\rm bol} = L_{\rm bol}/L_{1500} = 2$, in agreement with the galaxy templates used in the next section to evaluate the boost factor.

Figure 1 shows the cumulative and differential distributions of M_*, λ_E, and τ_{1500}. All of them span 3–4 dex, a range much larger than possible statistical and systematic errors, thus describing intrinsic galaxy properties. The distributions follow a power law at medium-high values but show a turnoff below a certain threshold due to the sample incompleteness at low M_*.

3. Dusty Outflows

We evaluate the boost factor A using CLOUDY (Ferland et al. 2013) and Starburst99 (Leitherer et al. 1999) simulations. We generate a large number of star-forming galaxy SEDs using Starburst99,[8] varying the SFR, stellar mass, metallicity, and age. We then use Cloudy to compute A, following Fabian et al. (2006). We found A in the range 450–600 for a 10–300 Myr starburst with $\mathrm{SFR} = 1$–$100 M_\odot\,\mathrm{yr}^{-1}$, $M_* = 10^7$–$10^8\,M_\odot$, metallicity $Z = 0.6$–$3\,Z_\odot$, and a Galactic dust-to-gas ratio $D = 1/162$. A reduces by ∼40%–45% if a 30% lower D value is adopted. Arakawa et al. (2022) calculate A for different dust grain compositions and sizes, finding values within the above ranges. At high optical depths, two additional competing effects enter in the determination of A. On one side, A depends linearly on the optical depth of the absorbing gas because gas shells located beyond $\tau_{1500} \gtrsim 1$ are not subject to radiation pressure. On the other side, in this regime, reprocessing of infrared radiation may further boost outflows (Ishibashi et al. 2018). The latter effect may be relevant for the galaxies with the highest densities ($N_{\rm H} > 10^{23}\mathrm{cm}^{-2}$, $\tau_{1500} > 50$), for which the infrared optical depth can exceed unity (Pallottini et al. 2017).

Sources in the outflow regime should be virtually dust free, and hence characterized by a small A_V, and blue UV spectral slopes ($\beta < -2$). On the contrary, systems that are not in that regime should be significantly attenuated by the dust produced by their stars. To test this basic hypothesis, in Figure 2 we plot τ_{1500} as a function of λ_E or the specific SFR (left panel) and the fraction of sources with $\tau_{1500} > 0.4$ (corresponding to 1 mag attenuation) as a function of λ_E (right panel).

The optical depth τ_{1500} decreases with λ_E following a power law with index -0.63 ± 0.10; the Spearman rank correlation coefficient is $R_{\rm SR} = -0.53$ for 132 degrees of freedom, with a Student distribution $t = 7.196$, implying a 100% probability of correlation. The correlation is even more significant ($R_{\rm SR} = -0.61$) if we exclude four sources (the starred symbols in Figure 2, left panel) for which Furtak et al. (2022) and Bradley et al. (2022) claim a Balmer break with $\mathcal{D}(4000) > 2$–3. Such a high $\mathcal{D}(4000)$ value is unlikely at high z because the time to grow such a Balmer break would be higher than the Hubble time (e.g., Maraston 2005; Noll et al. 2009). We also note an abrupt change in the fraction of obscured sources when crossing the $\lambda_E^{\rm eff} \approx 0.005$ line. Such fraction decreases from 80% for $\lambda_E \leqslant \lambda_E^{\rm eff}$ to ≈10% for larger values, where the outflow is predicted to occur.

As a next step, we investigate the frequency of galaxies developing a dusty outflow with redshift (Figure 3). From the left panel, we see that the Eddington ratio λ_E increases with redshift, implying that early galaxies present conditions more favorable to the onset of radiation-driven outflows. The relation has a slope of 2.1 ± 0.6, consistent with the Bouwens et al. (2022) determination. The Spearman rank correlation coefficient is 0.242, and the probability of correlation is 99.74%.

Interestingly, the fraction of galaxies developing an outflow according to the condition $\lambda_E > \lambda_E^{\rm eff}$ also increases with redshift, going from 20% at $z < 8.5$ to about 50% at $z = 8.5$–16. Thus, we conclude that a large fraction of the super-early galaxies detected by JWST are expected to have an outflow that has essentially emptied these systems of their interstellar medium.

4. Discussion

Despite early galaxies being complex systems, we have shown here that their observable properties are shaped by radiation-driven dusty outflows. Galaxies satisfying the outflow condition $\lambda_E > \lambda_E^{\rm eff}$ are much less extincted than galaxies with lower λ_E. Moreover, the fraction of galaxies with $\lambda_E > \lambda_E^{\rm eff}$, and thus candidates for hosting powerful dusty outflows, increases from about 20% at $z = 6.5$–8.5 to about 50% at

[7] ned.ipac.caltech.edu/level5/Sept12/Calzetti/Calzetti1_2.html
[8] https://www.stsci.edu/science/starburst99/docs/default.htm

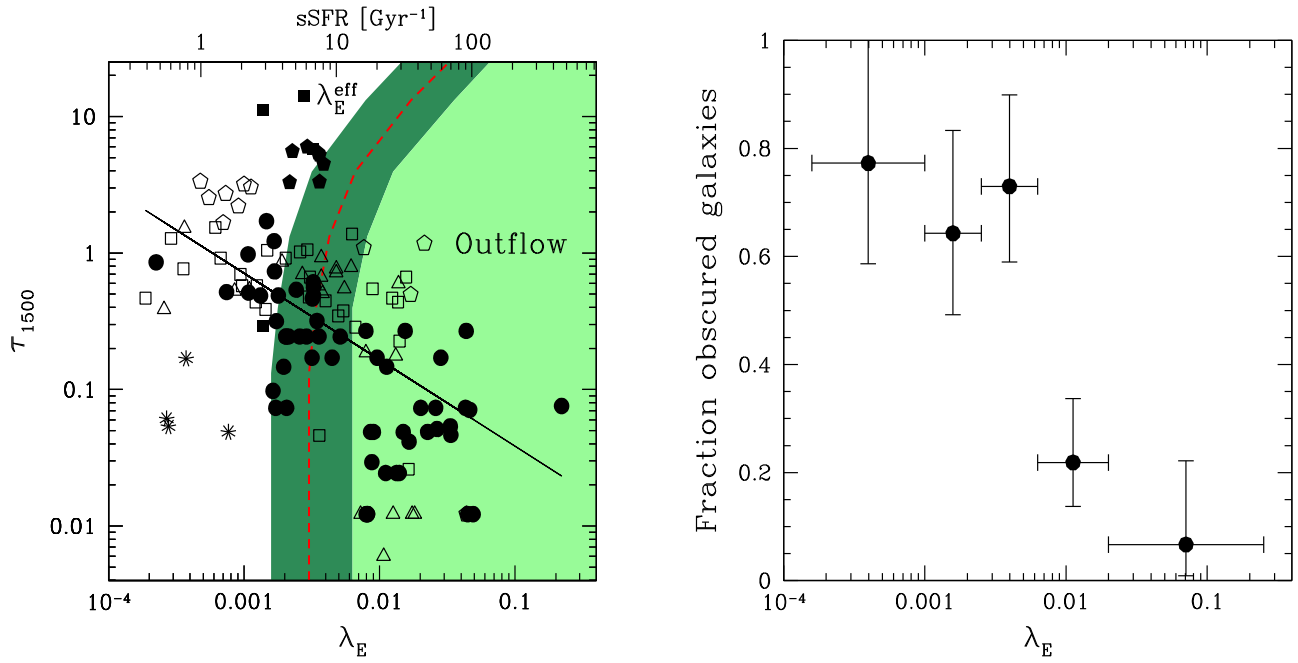

Figure 2. Left panel: dust UV optical depth vs. Eddington ratio (lower axis) and specific SFR (upper axis) for 134 galaxies at $z > 6.5$ in our sample. Filled circles are JWST-detected galaxy candidates from Bradley et al. (2022), Castellano et al. (2022), Curti et al. (2022), Finkelstein et al. (2022), Furtak et al. (2022), Harikane et al. (2022), Leethochawalit et al. (2023), Naidu et al. (2022), Topping et al. (2022), Trussler et al. (2022), and Whitler et al. (2022). Filled squares identify candidates from Rodighiero et al. (2022) and filled pentagons from Barrufet et al. (2022). Starred symbols are four sources from Furtak et al. (2022) and Bradley et al. (2022) for which the authors claim a Balmer break with $\mathcal{D}(4000) > 2$–3. Open squares are REBELS sources from Bouwens et al. (2022), open hexagons are REBELS sources with τ_{1500} estimated by Ferrara et al. (2022), and open triangles are Lyα emitters from Endsley et al. (2021). The solid line is the best-fit power law $\tau_{1500} \propto \lambda_E^{-0.63}$; also shown is the adopted functional form for $\lambda_E^{\rm eff}$ (red dashed), the range of likely values (dark green), and the outflow region (light and dark green). Right: fraction of galaxies with $\tau_{1500} > 0.4$ vs. Eddington ratio for our sample.

$z = 8.5$–16, confirming the sharp transition in galaxy properties proposed by Ziparo et al. (2022) at $z \simeq 8$ to explain the blue colors of JWST-detected super-early galaxies. Because the outflow occurs when the radiation pressure exceeds the gravitational pressure, the outflow velocity is greater than the escape velocity. Therefore, gas is inevitably lost from the galaxy in this scenario (even if it remained loosely bound, galaxies move, and thus gas would be stripped by ram pressure). This conclusion is supported by the recent ALMA dust continuum nondetections in three super-early galaxies (Bakx et al. 2022; Kaasinen et al. 2022; Popping 2022; Yoon et al. 2022). On the other hand, rejuvenation of the galaxy occurs both if gas falls back into the galaxy, as in the supernova-driven shock model by Nath et al. (2022), and by cosmological accretion of gas, restarting the SF. In the former case, obscuration is a transition phase, preceding and following the blowout phase. In the latter case, the accretion rate for a $10^{11} M_\odot$ halo at $z = 10$ is $\approx 280 M_\odot\,{\rm yr}^{-1}$. So, in 50–100 Myr the galaxy should return to a cosmological dark matter:baryon ratio.

The physical interpretation of the above results is straightforward if we assume that the observed UV luminosity is produced by star formation. First, recall that $\lambda_E \propto L_{\rm bol}/L_E$. As, in addition, $L_{\rm bol} \propto {\rm SFR}$ and $L_E \propto M_*$, it turns out that $\lambda_E \propto {\rm SFR}/M_* \equiv {\rm sSFR}$. Hence, the key parameter deciding whether a galaxy develops an outflow is the specific SFR. The outflow condition $\lambda_E > \lambda_E^{\rm eff}$ simply translates into the condition ${\rm sSFR} > {\rm sSFR}^* = 13\,{\rm Gyr}^{-1}$. It is interesting to note that the SFR densities of the high-z galaxies are between a few $M_\odot\,{\rm yr}^{-1}\,{\rm kpc}^{-2}$ and a few hundred $M_\odot\,{\rm yr}^{-1}\,{\rm kpc}^{-2}$ (assuming spherical symmetry and radii of the order of 100 pc), thus smaller than the Eddington-limited values in Diamond-Stanic et al. (2021) and Perrotta et al. (2021) (a few thousand $M_\odot\,{\rm yr}^{-1}\,{\rm kpc}^{-2}$).

It is useful to compare this specific SFR threshold with the predictions of numerical simulations for early galaxies. Pallottini et al. (2022; see their Figure 3) find that at $z \approx 8$, ${\rm sSFR} \simeq 100\,{\rm Gyr}^{-1}$ for young ($t_\star \lesssim 100$ Myr), small ($M_\star \lesssim 10^8 M_\odot$) galaxies and ${\rm sSFR} \sim 10\,{\rm Gyr}^{-1}$ for older ($t_\star \gtrsim 200$ Myr), more massive ($M_\star \gtrsim 10^9 M_\odot$) ones. Simulations by Kannan et al. (2022; see their Figure 5) show that ${\rm sSFR} \approx 10\,{\rm Gyr}^{-1}$ evolves very weakly from $z = 8$ to $z = 15$, and it is independent of stellar mass. We note that these simulations underpredict the abundance of luminous galaxies at $z > 10$, so their sSFR might be underestimated. Behroozi et al. (2019; their Figure 18) show that the average sSFR shows an increasing trend independently of the galaxy halo mass for $z \gtrsim 4$; interestingly, the curve crosses the sSFR* threshold at $z \approx 8$. Finally, Bouwens et al. (2022), by combining Hubble Ultra Deep Field and JWST NIRCam medium-band observations, find that $8 < z < 13$ galaxies have on average a high sSFR $\approx 24.5\,{\rm Gyr}^{-1}$. In spite of modeling and experimental uncertainties, it is clear that high-z galaxies are located very close to or above the sSFR* value required to drive an outflow. As a result, dusty outflows could be very common features in these systems.

The power-law shape of the bright end of the high-z galaxy UV luminosity function (Bowler et al. 2020; Donnan et al. 2022) suggests that BH accretion could substantially contribute to the UV luminosity of these systems. Indeed, at $z \sim 6$, the number density of galaxies in $-22 \leqslant M_{\rm UV} \leqslant -20$ (Bowler et al. 2020) is only a factor of a few higher than the active galactic nucleus (AGN) densities at the same magnitudes (Giallongo et al. 2019; Orofino et al. 2021), suggesting a high

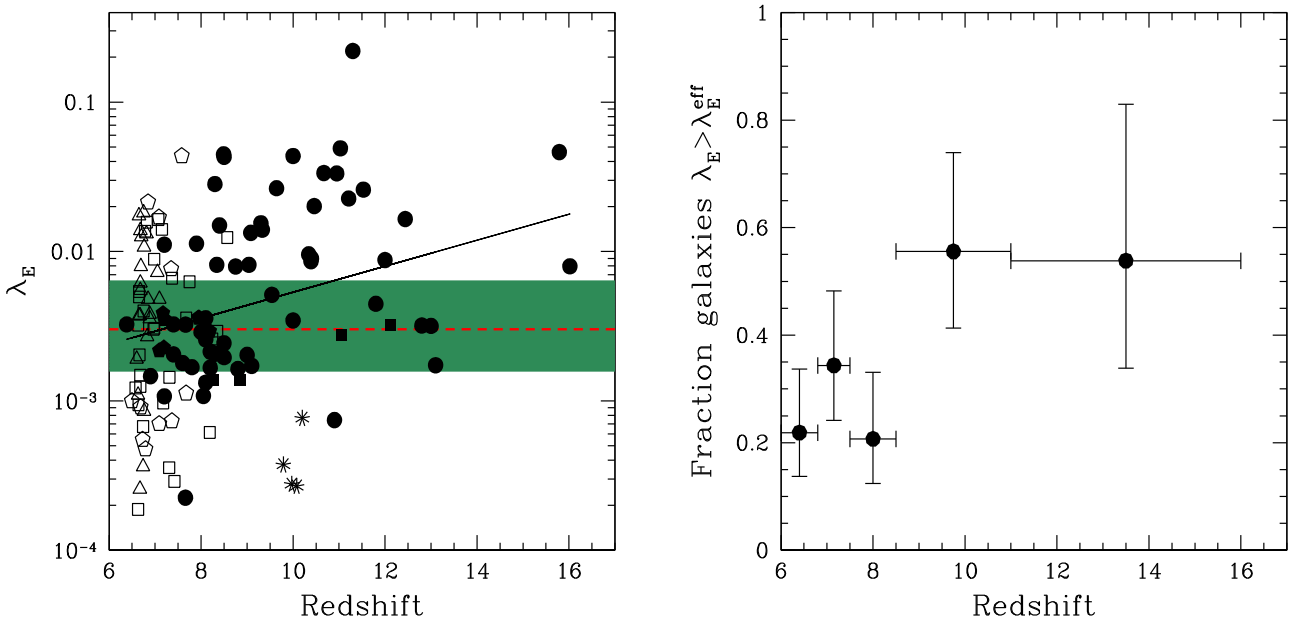

Figure 3. Left panel: redshift evolution of the Eddington parameter for the galaxies in the sample. Points are the same as in Figure 2. The solid line is the best-fit power law, $\lambda_E \propto (1+z)^{2.1}$. The red dashed line marks the optically thin value of $\lambda_E^{\rm eff}$ and the dark green region its most likely values. Right: fraction of galaxies satisfying the outflow condition $\lambda_E > \lambda_E^{\rm eff}$ vs. redshift.

AGN fraction at high z. This can be hard to assess using SED-fitting techniques, although claims of AGN detection in JWST data using such techniques do exist (Onoue et al. 2022). Reliable estimates of AGN fractions will be soon provided by JWST spectroscopy via the detection of N v lines and/or broad permitted lines in these systems. Furthermore, JWST spectroscopy could also provide observational evidence for outflows, allowing us to confirm and better quantify the scenario suggested in this Letter. If most of the luminosity of the brightest high-z galaxies is due to BH accretion, it requires BH masses $\approx 10^7$–$10^8 M_\odot$ accreting at rates closer to their Eddington luminosities. In this case, galaxy cleaning is mostly due to BH accretion rather than star formation.

Mechanical power can be provided to the outflow by supernova explosions. However, their contribution is likely to be subdominant as, due to the expected very high gas density in these systems, the explosion energy is rapidly radiated away[9] in a catastrophic cooling event (Pizzati et al. 2020). Similar conclusions concerning the inefficiency of supernova-driven outflows in early massive galaxies are presented in Bassini et al. (2022) and in the simulations of Nath et al. (2022), which find that the shock timescale to clean up a galaxy is two to five times longer than the SN dust production timescale. In the latter model, gas ejected by supernova-driven shocks can fall back into the galaxy, giving rise to a new obscured phase.

We acknowledge support from PRIN MIUR 2017 Black Hole Winds and the Baryon Life Cycle of Galaxies, 2017PH3WAT. A.F. acknowledges support from ERC Advanced Grant INTERSTELLAR H2020/740120. Generous support from the Carl Friedrich von Siemens-Forschungspreis der Alexander von Humboldt-Stiftung Research Award is kindly acknowledged (A.F.).

Facilities: HST, JWST.

software: astropy (Astropy Collaboration et al. 2013), CLOUDY (Ferland et al. 2013), Starburst99 (Leitherer et al. 1999).

[9] For example, for the typical values of $M_* \approx 10^9\ M_\odot$, $r_e = 100$ pc, and assuming a gas fraction $f_g = M_g/(M_g + M_*) \gtrsim 0.5$, appropriate for high-$z$ galaxies, we obtain a mean gas density $n \gtrsim 10^4$. In these conditions, free–free cooling would cause the supernova blast to become radiative after ≈100 yr, thus dramatically quenching its propagation (Terlevich et al. 1992; Jiménez et al. 2019).

ORCID iDs

Fabrizio Fiore https://orcid.org/0000-0002-4031-4157
Andrea Ferrara https://orcid.org/0000-0002-9400-7312
Manuela, Bischetti https://orcid.org/0000-0002-4314-021X
Chiara Feruglio https://orcid.org/0000-0002-4227-6035
Andrea Travascio https://orcid.org/0000-0002-8863-888X

References

Adams, N. J., Conselice, C. J., Ferreira, L., et al. 2023, MNRAS, 518, 4755
Arakawa, N., Fabian, A. C., Ferland, G. J., & Ishibashi, W. 2022, MNRAS, 517, 5069
Arav, N., Li, Z.-Y., & Begelman, M. C. 1994, ApJ, 432, 62
Astropy Collaboration, Robitaille, T. P., Tollerud, E. J., et al. 2013, A&A, 558, A33
Bakx, T. J. L. C., Zavala, J. A., Mitsuhashi, I., et al. 2023, MNRAS, 519, 5076
Barrufet, L., Oesch, P. A., Weibel, A., et al. 2022, arXiv:2207.14733
Bassini, L., Feldmann, R., Gensior, J., et al. 2022, arXiv:2211.08423
Behroozi, P., Wechsler, R. H., Hearin, A. P., & Conroy, C. 2019, MNRAS, 488, 3143
Bouwens, R. J., Stefanon, M., Brammer, G., et al. 2022, arXiv:2211.02607
Bowler, R. A. A., Jarvis, M. J., Dunlop, J. S., et al. 2020, MNRAS, 493, 2059
Bradley, L. D., Coe, D., Brammer, G., et al. 2022, arXiv:2210.01777
Castellano, M., Fontana, A., Treu, T., et al. 2022, ApJL, 938, L15
Chevallard, J., & Charlot, S. 2016, MNRAS, 462, 1415
Curti, M., D'Eugenio, F., Carniani, S., et al. 2022, MNRAS, 518, 425
Diamond-Stanic, A. M., Moustakas, J., Sell, P. H., et al. 2021, ApJ, 912, 11
Donnan, C. T., McLeod, D. J., Dunlop, J. S., et al. 2023, MNRAS, 518, 6011
Endsley, R., Stark, D. P., Charlot, S., et al. 2021, MNRAS, 502, 6044
Fabian, A. C., Celotti, A., & Erlund, M. C. 2006, MNRAS, 373, L16
Fabian, A. C., Vasudevan, R. V., & Gandhi, P. 2008, MNRAS, 385, L43
Ferland, G. J., Porter, R. L., van Hoof, P. A. M., et al. 2013, RMxAA, 49, 137
Ferrara, A., Ferrini, F., Barsella, B., & Aiello, S. 1990, A&A, 240, 259
Ferrara, A., Pallottini, A., & Dayal, P. 2022, arXiv:2208.00720

Finkelstein, S. L., Bagley, M. B., Arrabal Haro, P., et al. 2022, ApJ, 940, 55
Furtak, L. J., Shuntov, M., Atek, H., et al. 2023, MNRAS, 519, 3064
Giallongo, E., Grazian, A., Fiore, F., et al. 2019, ApJ, 884, 19
Harikane, Y., Ouchi, M., Oguri, M., et al. 2022, arXiv:2208.01612
Ishibashi, W., Fabian, A. C., Ricci, C., & Celotti, A. 2018, MNRAS, 479, 3335
Jiménez, S., Tenorio-Tagle, G., & Silich, S. 2019, MNRAS, 488, 978
Kaasinen, M., van Marrewijk, J., Popping, G., et al. 2022, arXiv:2210.03754
Kannan, R., Springel, V., Hernquist, L., et al. 2022, arXiv:2210.10066
Krumholz, M. R., & Thompson, T. A. 2012, ApJ, 760, 155
Krumholz, M. R., & Thompson, T. A. 2013, MNRAS, 434, 2329
Leethochawalit, N., Trenti, M., Santini, P., et al. 2023, ApJL, 942, L26
Leitherer, C., Schaerer, D., Goldader, J. D., et al. 1999, ApJS, 123, 3
Maraston, C. 2005, MNRAS, 362, 799
Murray, N., Quataert, E., & Thompson, T. A. 2005, ApJ, 618, 569
Naidu, R. P., Oesch, P. A., Setton, D. J., et al. 2022, arXiv:2208.02794
Nath, B. B., Vasiliev, E. O., Drozdov, S. A., & Shchekinov, Y. A. 2022, arXiv:2211.12378
Noll, S., Burgarella, D., Giovannoli, E., et al. 2009, A&A, 507, 1793
Ono, Y., Harikane, Y., Ouchi, M., et al. 2022, arXiv:2208.13582
Onoue, M., Inayoshi, K., Ding, X., et al. 2023, ApJ, 942, 17
Orofino, M. C., Ferrara, A., & Gallerani, S. 2021, MNRAS, 502, 2757
Pallottini, A., Ferrara, A., Gallerani, S., et al. 2017, MNRAS, 465, 2540
Pallottini, A., Ferrara, A., Gallerani, S., et al. 2022, MNRAS, 513, 5621
Perrotta, S., George, E. R., Coil, A. L., et al. 2021, ApJ, 923, 275
Pizzati, E., Ferrara, A., Pallottini, A., et al. 2020, MNRAS, 495, 160
Popping, G. 2023, A&A, 669, 8
Reddy, N. A., Oesch, P. A., Bouwens, R. J., et al. 2018, ApJ, 853, 56
Ricci, C., Trakhtenbrot, B., Koss, M. J., et al. 2017, Natur, 549, 488
Rodighiero, G., Bisigello, L., Iani, E., et al. 2023, MNRAS, 518, 18
Scoville, N. Z., Polletta, M., Ewald, S., et al. 2001, AJ, 122, 3017
Terlevich, R., Tenorio-Tagle, G., Franco, J., & Melnick, J. 1992, MNRAS, 255, 713
Thompson, G. D., Speck, A. K., & Dijkstra, C. 2005, AAS Meeting Abstracts, 207, 182.07
Thompson, T. A., Fabian, A. C., Quataert, E., & Murray, N. 2015, MNRAS, 449, 147
Topping, M. W., Stark, D. P., Endsley, R., et al. 2022, MNRAS, 516, 975
Trussler, J. A. A., Adams, N. J., Conselice, C. J., et al. 2022, arXiv:2207.14265
Whitler, L., Endsley, R., Stark, D. P., et al. 2023, MNRAS, 519, 5859
Yang, L., Leethochawalit, N., Treu, T., et al. 2022, MNRAS, 514, 1148
Yoon, I., Carilli, C. L., Fujimoto, S., et al. 2022, arXiv:2210.08413
Ziparo, F., Ferrara, A., Sommovigo, L., & Kohandel, M. 2022, arXiv:2209.06840